Evaluation of the MODIS Aerosol Retrievals over Ocean and Land during CLAMS

R. C. Levy, L. A. Remer, J. Martins, Y. J. Kaufman, Artemio Plana-Fattori, J. Redemann, B. Wenny

Evaluation of the MODIS Aerosol Retrievals over Ocean and Land during CLAMS

R. C. LEVY,[*,+] L. A. REMER, J. V. MARTINS,[#] AND Y. J. KAUFMAN

Laboratory for Atmospheres, NASA Goddard Space Flight Center, Greenbelt, Maryland

A. PLANA-FATTORI[@]

GEST, University of Maryland, Baltimore County, Baltimore, and NASA Goddard Space Flight Center, Greenbelt, Maryland

J. REDEMANN

Bay Area Environmental Research Institute, Sonoma, and NASA Ames Research Center, Moffett Field, California

B. WENNY

SAIC, and NASA Langley Research Center, Hampton, Virginia

(Manuscript received 4 September 2003, in final form 29 June 2004)

ABSTRACT

The Chesapeake Lighthouse Aircraft Measurements for Satellites (CLAMS) experiment took place from 10 July to 2 August 2001 in a combined ocean–land region that included the Chesapeake Lighthouse [Clouds and the Earth's Radiant Energy System (CERES) Ocean Validation Experiment (COVE)] and the Wallops Flight Facility (WFF), both along coastal Virginia. This experiment was designed mainly for validating instruments and algorithms aboard the *Terra* satellite platform, including the Moderate Resolution Imaging Spectroradiometer (MODIS). Over the ocean, MODIS retrieved aerosol optical depths (AODs) at seven wavelengths and an estimate of the aerosol size distribution. Over the land, MODIS retrieved AOD at three wavelengths plus qualitative estimates of the aerosol size. Temporally coincident measurements of aerosol properties were made with a variety of sun photometers from ground sites and airborne sites just above the surface. The set of sun photometers provided unprecedented spectral coverage from visible (VIS) to the solar near-infrared (NIR) and infrared (IR) wavelengths. In this study, AOD and aerosol size retrieved from MODIS is compared with similar measurements from the sun photometers. Over the nearby ocean, the MODIS AOD in the VIS and NIR correlated well with sun-photometer measurements, nearly fitting a one-to-one line on a scatterplot. As one moves from ocean to land, there is a pronounced discontinuity of the MODIS AOD, where MODIS compares poorly to the sun-photometer measurements. Especially in the blue wavelength, MODIS AOD is too high in clean aerosol conditions and too low under larger aerosol loadings. Using the Second Simulation of the Satellite Signal in the Solar Spectrum (6S) radiative code to perform atmospheric correction, the authors find inconsistency in the surface albedo assumptions used by the MODIS lookup tables. It is demonstrated how the high bias at low aerosol loadings can be corrected. By using updated urban/industrial aerosol climatology for the MODIS lookup table over land, it is shown that the low bias for larger aerosol loadings can also be corrected. Understanding and improving MODIS retrievals over the East Coast may point to strategies for correction in other locations, thus improving the global quality of MODIS. Improvements in regional aerosol detection could also lead to the use of MODIS for monitoring air pollution.

[*] Additional affiliation: Science Systems and Applications, Inc., Lanham, Maryland.
[+] Additional affiliation: Department of Meteorology, University of Maryland, College Park, College Park, Maryland.
[#] Additional affiliation: Joint Center for Earth Systems Technology, University of Maryland, Baltimore County, Baltimore, Maryland.
[@] Permanent affiliation: Institute of Astronomy, Geophysics and Atmospheric Sciences, University of São Paulo, São Paulo, Brazil.

Corresponding author address: Mr. Robert Levy, Code 913, NASA Goddard Space Flight Center, Greenbelt, MD 20771.
E-mail: levy@climate.gsfc.nasa.gov

1. Introduction

Tropospheric aerosols significantly influence the global energy balance and the hydrological cycle (Houghton et al. 2001). They scatter solar radiation back to space, absorb both solar and terrestrial radiation, and act as cloud condensation nuclei (CCN), influencing cloud/precipitation processes and changing cloud reflectivity. Sometimes known as suspended airborne particles, or particulate matter (PM), aerosols are a component of local smog and regional air pollution (Chen et al. 2002; Dickerson et al. 1997). Aerosols reduce aesthetic visibility (Malm 1992) and adversely affect human health (Samet et al. 2000). To people living along the East Coast of the United States, air pollution is a major concern, especially during the summer months (e.g., Kaufman and Fraser 1983; Malm 1992). Because aerosols are not well mixed in the atmosphere, (i.e., they are spatially and temporally inhomogeneous), new tools have been developed to begin to understand aerosol interactions and transport processes on many scales.

One of these new sensors is the Moderate Resolution Imaging Spectroradiometer (MODIS; King et al. 1992; King et al. 2003), which has been flying aboard the National Aeronautics and Space Administration's (NASA) *Terra* spacecraft since December 1999, and NASA's *Aqua* spacecraft beginning in May 2002 (Parkinson 2003). This satellite instrument offers near-global coverage on a daily basis, with fine spatial and spectral resolution. MODIS measures radiance at 250 m to 1 km, in 36 channels spanning the spectral range from 0.44 to 15 μm. Aerosol retrieval makes use of seven solar spectral channels (0.47–2.1 μm) at 250- and 500-m spatial resolution (Tanré et al. 1997; Kaufman et al. 1997b; Levy et al. 2003). Cloud identification and masking make use of many of the same solar wavelengths, but also include tests using other solar channels and longer IR (terrestrial) channels (Platnick et al. 2003; Martins et al. 2002; Gao et al. 2002). Because of the wide spectral range, MODIS can measure aerosol optical depth over both ocean and land and provide quantitative estimates of aerosol size (Tanré et al. 1996). Because of the high spatial resolution, MODIS can provide informative assessments of inhomogeneous aerosol events, with unprecedented proximity to clouds.

Previous validation exercises have shown that, globally, MODIS aerosol optical depth (AOD or τ) and aerosol size products can be compared with AOD and size retrievals from ground-based sun photometers. Over nondust oceanic areas near coastal or island Aerosol Robotic Network (AERONET) sites (Holben et al. 1998), the MODIS AOD fits AERONET AOD with remarkable accuracy; $R \approx 0.95$ and the offsets and slopes are near zero and one, respectively (Remer et al. 2002; Remer et al. 2005). The size retrieval also shows some skill, where nearly two-thirds of the effective radii retrievals fall within ± 0.11 μm (Remer et al. 2005). In dusty regions, however, MODIS misrepresents the spectral dependence of the AOD, and thus the aerosol size retrieval (Levy et al. 2003). Over land, MODIS and AERONET compare within prelaunch expectations (two-thirds of the points are within $\Delta\tau = \pm 0.15 \pm 0.05\tau$), but generally MODIS overestimates AOD for low aerosol loadings and underestimates for high loadings (Chu et al. 2002; Remer et al. 2005). For coastal sites, where both land and ocean products can be compared with AERONET separately, MODIS imagery sometimes shows discontinuous AOD from ocean to land. Global, long-term scatterplots of AOD and effective radii are informative, but they may hide systematic errors pertaining to certain regions. Remer et al. (2005) separated the global scatterplot into a number of large regions, presumably each region representing a given aerosol regime. Some of the poorest MODIS–AERONET comparisons were over the land along the East Coast of the United States, where less than 60% of the retrievals fell within expected error bars (between 2000 and 2002). This was the primary motivation to perform detailed analysis of MODIS products along the East Coast of the United States.

The Chesapeake Lighthouse and Aircraft Measurements for Satellites (CLAMS) experiment (Smith et al. 2005) was designed in part to examine and validate satellite retrievals of atmospheric properties over coastlines. CLAMS was organized by NASA's Earth Observing System team members and included representation from many *Terra* instruments (including MODIS), plus a number of surface and aircraft groups. Intensive ground-based observations were performed at Wallops Flight Facility (WFF) at Chincoteague, Virginia, and also at the Chesapeake Lighthouse [Clouds and the Earth's Radiant Energy System (CERES) Ocean Validation Experiment (COVE)], some 14 km off the Norfolk, Virginia, coastline. Held in July and August 2001, it was expected that CLAMS would showcase the heavy aerosol loadings common to the U.S. East Coast during the summer. The CLAMS surface and aircraft campaigns provided an unprecedented density of potentially useful comparisons of sun-photometer data to MODIS, providing data to evaluate MODIS aerosol products over both ocean and land. Specifically, this extensive dataset also could be used to provide insight into the generally poor U.S. East Coast land comparisons that were introduced in Remer et al. (2005).

In section 2, we provide a brief introduction to the MODIS aerosol algorithms and products, paying special attention to concepts discussed in this paper. Section 3 describes the CLAMS instrumentation and data used for this study. Section 4 shows MODIS–sun photometer comparisons for both spectral AOD and size retrievals, for both ocean and land. This includes a comparison of aerosol size distributions for each of the different retrievals. In section 5, we attempt to show how

aerosol retrievals over the CLAMS region can be improved in the future, focusing separately on aerosol model and surface reflectance issues. Finally, section 6 summarizes and provides pathways for future study.

2. MODIS

The MODIS aerosol algorithm is actually two entirely independent algorithms, one to derive aerosol properties over land surfaces, the second for over the ocean. Both algorithms were conceived and coded prior to *Terra* launch (Kaufman et al. 1997b; Tanré et al. 1997), and scientifically have changed little since then. However, some of the mechanics and details have evolved and have been the focus of studies, such as those done by Levy et al. (2003) and Ichoku et al. (2003). Reflected solar and emitted terrestrial radiances are observed by MODIS at 250 m, 500 m, or 1 km, along a swath 2330 km wide. These data are collected in 5-min chunks, called a granule, each about 1350 km along track. Normally, 288 of these granules are collected in one day, and about 135 have enough reflected sunlight to be useful for aerosol retrieval. Calibrated reflectance data products at multiple resolutions (MOD02) plus geolocation (MOD03) are called level 1B (L1B). The primary geophysical products [known as level 2 (L2)] include the MODIS cloud mask (MOD35) and atmospheric profile (MOD07) products (Platnick et al. 2003), both required prior to aerosol retrieval. These L1B and L2 products, plus ancillary data (such as water vapor profiles), comprise the set of inputs to the MODIS aerosol retrieval.

The aerosol retrieval uses calibrated reflectance data from the first seven MODIS bands (between 0.47 and 2.1 μm). These reflectance data are first corrected for trace gas and water vapor columns, using climatology for ozone and the National Centers for Environmental Prediction (NCEP) ancillary data for column water vapor (see the ATBD link on the Web site http://modisland.gsfc.nasa.gov/mod09/).

Of the seven MODIS bands, two channels (0.66 and 0.86 μm) are measured with 250-m resolution, whereas the other five (0.47, 0.55, 1.24, 1.64, and 2.13 μm) are at 500 m. The final aerosol retrieval is for 10 km $\times$ 10 km, requiring aggregation from the higher resolution channels (i.e., 40 $\times$ 40 for the 250-m channels, and 20 $\times$ 20 for the 500-m channels). Using results from the geolocation and cloud mask data, the individual pixels in the level 1B granule are classified as ocean or land. If all pixels in the 10 km $\times$ 10 km box are determined to be "ocean," then the ocean algorithm is performed. If any pixel is land, then the land retrieval is applied. Even though MODIS was operational during the CLAMS period (July–August 2001), this study uses data retrieved using a more modern version (known as V4.1.3). Remer et al. (2005) places V4.1.3 in historical context since inception in 1997 and includes many details that are covered here.

After the land or ocean branch is concluded, the algorithm merges some parameters into combined land and ocean products for convenience. The main combined land–ocean products are the AOD at 0.55 μm and the fine-mode weighting (FMW). The FMW is the fraction of the total AOD at 0.55 μm that was contributed by smaller particles. Note that the land and ocean retrievals are not required to meet at the shoreline, and may be discontinuous. Additional products are operationally derived as "retrieved" or "diagnostic" parameters and are detailed in Remer et al. (2004).

a. MODIS over ocean

If all pixels in the 10 km $\times$ 10 km box are identified as water pixels, the ocean algorithm is chosen. First, "obstructed" pixels (cloudy or otherwise unsuitable for retrieval) are removed, including those within the glint mask (within 40° of the specular reflection angle), those flagged as cloudy (Platnick et al. 2003; Martins et al. 2002; Gao et al. 2002), and those that contain suspended river or other sediments (Li et al. 2003). The remaining good pixels are sorted by their near-infrared (NIR) (0.86 μm) brightness. Of these, the darkest and brightest 25% are removed, thereby eliminating residual cloud and/or surface contamination. If at least 10 pixels remain in the 10 km $\times$ 10 km box, then reflectance statistics for all seven channels are calculated and used for the inversion.

As introduced by Tanré et al. (1997) and updated by Levy et al. (2003) and Remer et al. (2005), the MODIS inversion attempts to minimize the difference between the observed spectral radiance in six MODIS channels and radiance precomputed in a lookup table. The lookup table models the total reflectance observed by satellite, which includes not only aerosol contributions, but also spatially and temporally constant atmospheric (Rayleigh) and ocean surface (chlorophyll, foam, whitecaps, and sun glint) contributions. The aerosol radiance contribution is computed for 2304 sun/surface/satellite geometries and five total aerosol loadings, for four fine modes and five coarse modes [see Levy et al. (2003) or Remer et al. (2005) for more details]. The inversion uses the observed geometry and assumes that the total aerosol contribution is composed of a single fine and single coarse mode. Upon finding best fits to the observed reflectance, the algorithm reports the total AOD, the FMW to the total AOD, and the modes chosen. A variety of other aerosol parameters are then inferred, including spectral optical thickness and effective radius of the size distribution.

b. MODIS over land

Like the over-ocean algorithm, the theoretical retrieval has not changed much since its inception (Kaufman et al. 1997b). However, for version V4.1.3, new masks for clouds and ice/snow have been added, along with improved aerosol models for African biomass-burning regions (Remer et al. 2005).

Not all pixels in the 10 km × 10 km box need to be detected as land for the land retrieval to continue. First, cloudy pixels are removed by combining cloud mask tests (Platnick et al. 2003; Martins et al. 2002; Gao et al. 2002). The Normalized Difference Vegetation Index (NDVI) discards large water bodies (lakes, rivers) and most snow or ice pixels. From the remaining pixels, the algorithm selects "dark" surface pixels, based on the reflectance at 2.1 μm. These dark pixels are sorted, according to reflectance in the red (0.66 μm). The darkest 20% and brightest 50% of the dark pixels are discarded, statistically skewed to selectively eliminate pixels contaminated by clouds, cloud shadows, or odd surfaces. The remaining 30% of the pixels are used in the aerosol retrieval.

If at least 12 pixels (less are allowed but with caveats) remain in the 10 km × 10 km box, the algorithm calculates the mean measured reflectance at the three land wavelengths (0.47, 0.66, and 2.1 μm). Using empirical relationships proposed by Kaufman et al. (1997c), and theoretically examined in Kaufman et al. (2002), the surface reflectance in the two visible (VIS) wavelengths are estimated from the reflectance at 2.1 μm. The difference between the surface reflectance and the Rayleigh (standard atmosphere)-corrected satellite reflectance is known as the aerosol "path reflectance." Assuming a generic, mostly fine mode "continental aerosol" model (which includes three modes; e.g., Kaufman et al. 1997b), the MODIS-measured path reflectance is compared with reflectance found in precomputed lookup tables (which include effects of geometry and aerosol absorption). AOD is derived at 0.47 and 0.66 μm independently.

The spectral dependence of the path reflectance, determined from the preliminary use of the continental aerosol model, determines whether to add coarse dust (Kaufman et al. 1997b). Then, the fine model is rederived using a specific aerosol model, depending on the season and location [all models are described in Remer et al. (2005)]. For retrievals over the CLAMS region and season, the "urban/industrial" aerosol model (Remer and Kaufman 1998) is the appropriate choice for the fine model. Like the over-ocean algorithm, a number of aerosol products are inferred, including the AOD and a qualitative parameter analogous to the FMW at 0.55 μm.

c. MODIS aerosol validation

The primary means of validating MODIS aerosol parameters is by comparison with AERONET ground sun-photometer data. These instruments measure spectral AOD to within 0.01 (Holben et al. 1998; Eck et al. 1999) and can derive ambient, total atmospheric column aerosol size distributions and effective radius assuming spherical particles (Dubovik and King 2000). Assuming that temporally varying sun-photometer data can be compared with spatially varying satellite data, we use the validation methodology described by Ichoku et al. (2002a). Sun-photometer measurements between ±30 min of overpass are compared with MODIS measurements between ±25 km of the sun-photometer site. The resulting 50 km × 50 km MODIS box is made up twenty-five 10 km × 10 km aerosol retrievals, which may be over ocean or land, and in coastal regions (such as CLAMS) may include both. If retrievals are made over both surfaces, then both values are compared with the sun-photometer data. As the aerosol algorithms have been continually updated since *Terra* launch, validation is an ongoing effort.

Preliminary validation of the aerosol products was made from MODIS during the first few months of operation and showed that MODIS-derived parameters including AOD and effective radius compared favorably with AERONET data (Ichoku et al. 2002a; Remer et al. 2002; Chu et al. 2002). Validation of MODIS data through August 2002 (Remer et al. 2005) demonstrated that for both over ocean and land, about two-thirds of MODIS AOD retrievals fell within expected uncertainty ($\pm 0.03 \pm 0.05\tau$ over ocean and $\pm 0.05 \pm 0.15\tau$ over land). Additionally, over the ocean, 66% of MODIS effective radius retrievals were within ±0.11 μm of the AERONET-derived values (Remer et al. 2002; Remer et al. 2005).

Yet, whereas AODs over land mostly fit within uncertainty lines, there was a generally positive AOD offset at low optical depths, and AOD underestimation at larger optical depths. At the blue wavelength, this phenomenon was especially pronounced for the "East US_land" region, where less than 60% of the AOD retrievals were within the expected uncertainties (Remer et al. 2005). Retrievals over the nearby ocean were more accurate and consistent with the global ocean comparisons. Indeed, images of AOD along the East Coast often show discontinuities. Additionally, a major weakness of the previous MODIS studies was the lack of spectral comparison at the longer wavelengths. AERONET provides AOD measurements only in the visible and near-IR wavelengths.

3. CLAMS instrumentation and data

The CLAMS experiment, sponsored by NASA's Earth Observing System (EOS) Science Team, was the first combined validation of the sensors aboard *Terra* (Smith et al. 2005). CLAMS was held 10 July to 2 August 2001, at NASA's Wallops Flight Facility near Chincoteague, Virginia. The activities included five instrumented aircraft and intensive ground sites on and around the WFF and the Chesapeake Lighthouse (14 km off the coast of Norfolk, Virginia). Additionally, a number of nearby AERONET and other sun-photometer sites were operated, some providing AOD into the IR wavelengths.

a. MODIS during CLAMS

The MODIS data used in this study were processed during the MODIS "reprocessing" effort of 2003, using the V4.1.3 aerosol algorithms implemented in late 2002 (described by Remer et al. 2005). Table 1 shows MODIS overpass dates/times and whether the CLAMS region was outside of the MODIS glint mask ($> 40°$) and potentially available for aerosol retrieval over ocean. The two columns marked "Land" or "Ocean" denote whether over-land or over-ocean retrievals from this granule were used in sun-photometer comparisons. MODIS data were used only when there were at least five pixels available (within the 50 km $\times$ 50 km box).

b. Sun photometers

Many different types of sun photometers measured spectral AOD during CLAMS. AERONET (Holben et al. 1998) sun photometers (manufactured by Cimel Electronique, France) operated at a number of sites in the region, automatically providing consistent AOD measurements. Two additional robotic sun photometers (described in Ehsani et al. 1998) were operated side-by-side at NASA Langley Research Center (LaRC) on clear days. The Ames Airborne Tracking Sun-photometer-14 Channel (AATS-14) flew aboard the University of Washington's Convair 580 aircraft (Redemann et al. 2005; Russell et al. 1993). In addition, six Microtops II portable, handheld sun photometers (Morys et al. 2001) were deployed at multiple locations and times during CLAMS. All sun photometers used in this study were pre- and/or postcalibrated for CLAMS and were expected to measure optical depths within ± 0.03 (see Holben et al. 1998; Ichoku et al. 2002b; Rus-

TABLE 1b. Key for reading Table 1a. Each sun-photometer site is listed, along with a code and its latitude and longitude.

Key Sunphotometer Locations used for MODIS comparisons			
Code	Location	Longitude (°)	Latitude (°)
AERONET			
A1	COVE	−75.7	36.9
A2	GSFC	−76.88	39.03
A3	GISS	−73.96	40.798
A4	MD_Science	−76.617	39.283
A5	Oyster	−75.933	37.295
A6	Wallops	−75.48	37.94
A7	SERC	−76.5	38.883
A8	Philadelphia	−75.005	40.036
Microtops			
M1	Assateague	−75.35	37.88
M2	Assawoman	−75.38	37.87
M3	Chincoteague	−75.38	37.92
M4	COVE_MTOPS	−75.7	36.9
M5	Nash_Corner	−75.54	37.95
M6	Wallops_Chem	−75.49	37.83
M7	Wallops_Hangar	−75.47	37.94
LaRC			
L1	LaRC	−76.379	37.105
AATS-16			
T1	AATS0714	−75.731	36.907
T2	AATS0723	−74.113	37.866
T3	AATS0731	−70.416	38.471

TABLE 1a. Collocated sun-photometer data potentially available to compare with MODIS over land and/or ocean retrievals. Actual compared data will be reduced due to cloud screening and other filtering. "In glint" refers to whether COVE is within the MODIS glint mask (glint angle $< 40°$). The sun-photometer code key is shown in Table 1b.

Terra (over COVE)			Sun-photometer data	
Date	Time (UTC)	In glint?	Land	Ocean
10 Jul 2001	1606	Yes	A7, A2, M1, M2, M3, M5, L1	
11 Jul 2001	1648	No		
12 Jul 2001	1553	No	A8, M1, L1	A1, L1
13 Jul 2001	1636	Yes	A7, A8, A4, A2	
14 Jul 2001	1541	No	A7, A8, A5, A2, A1, M6, T1	A1, M6, T1
15 Jul 2001	1624	Yes	A8, A4, A2, A3	
16 Jul 2001	1529	No	A6, A8, A3, M1, M2, M5, L1	A6, M1, M2, M5
17 Jul 2001	1612	Yes	M1, M2, M5, L1	
18 Jul 2001	1517	No		
19 Jul 2001	1600	Yes		
20 Jul 2001	1642	Yes	A8, A4, A3	
21 Jul 2001	1547	No	A6, A7, A8, A4, A2, A1, M3, M7	A1, M3, M7
22 Jul 2001	1630	Yes	A6, A7, A2, A8, A3, M7	
23 Jul 2001	1535	No	A8, A3, M3, M7	A1, M3, M7, T2
24 Jul 2001	1618	Yes		
25 Jul 2001	1523	No	A8, M4, M6	A6, A5, A1, M4, M6
26 Jul 2001	1606	Yes		
27 Jul 2001	1648	Yes	A6, A8, A8, A3	
28 Jul 2001	1554	No		
29 Jul 2001	1636	Yes		
30 Jul 2001	1541	No		
31 Jul 2001	1624	Yes	A6, A8, A5, A3, A1, M5, M6	T3
1 Aug 2001	1529	No	A6, A7, A5, A4, A2, A3, A1, M1, M5, M6	A6, A5, A1, M1, M5, M6
2 Aug 2001	1612	Yes	A6, A7, A8, A5, A4, A2, A3, M1, M6	

sell et al. 1993; and Ehsani et al. 1998 for accuracy details). The AERONET instruments have the additional capability of retrieving aerosol size and optical parameters using almucantur radiance measurements (Dubovik and King 2000).

CLAMS was the first major field experiment to have potential MODIS validation in longer wavelengths (including 2.1 μm), in addition to the visible and NIR channels on AERONET and standard Microtops instruments. The AERONET Cimels measured only between 0.34 and 1.02 μm. Both the LaRC sun photometers and the AATS-14 (Redemann et al. 2005) measured out to 1.55 μm, while customized Microtops instruments added 1.6- and 2.1-μm channels. Details for calibration and deployment of the customized Microtops are given in appendix A.

Figure 1 is a map of the CLAMS experiment, depicting deployment locations for the sun photometers in the immediate region. Different instrument types are denoted by different colors/shapes. Table 1 indicates which sun photometers (and locations) were used to compare with MODIS data. References to MODIS comparable sun-photometer data are found under the columns "Ocean" and "Land." Table 1a provides the key to the sun-photometer types and site names, along with their latitude–longitude coordinates. Cimels are named according to the AERONET database, and the Microtops are referred to by instrument number and deployed location. There were two LaRC instruments located side-by-side at NASA Langley, but their data were combined here. For the AATS-14 data, we list the 10 flights that included straight runs less than 100 m from the ocean surface and within a few minutes of MODIS overpass. The locations and times in Table 1 represent the approximate locations of the AATS-14 measurements during overpass.

Figure 2 shows a cloud-screened and calibrated level 2 (Smirnov et al. 2000) time series of AOD from two AERONET locations (Wallops and COVE) during CLAMS. Data are not screened as to the number of points measured in a day, meaning that residual cloud contamination (even after stringent cloud screening) may still be an issue. The AOD spikes on 19 July (day 200) and 11 July (day 192) are likely cloud contamination; 17 July (day 198) was considered the CLAMS "golden day" because of relatively high AOD (around 0.5–0.7 at 0.55 μm) measured at both stations. Unfortunately, this day is useless for operational MODIS over-ocean comparison because the region was within the glint (see Table 1). On other days with lower AOD, MODIS can be compared to AERONET data.

4. MODIS comparison with sun photometers

As a result of previous studies (such as Levy et al. 2003) we assumed that the AERONET, Microtops ("classic" channels), and AATS sun-photometer data were consistent with each other during CLAMS. We further assumed that data from the LaRC sun photometers and properly calibrated customized Microtops

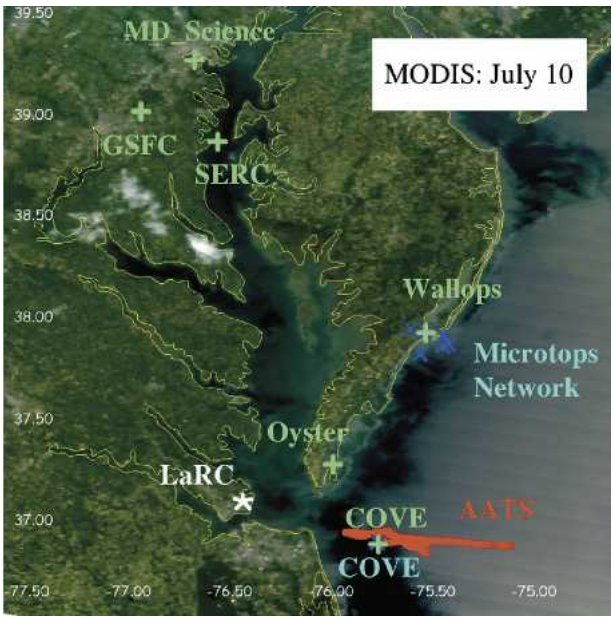

FIG. 1. Map of sun-photometer sites during CLAMS. Blue, green, and white represent the Microtops network, AERONET, and the LaRC sites, respectively. The red is the track of the AATS-14 on 17 Jul 2001 (as an example).

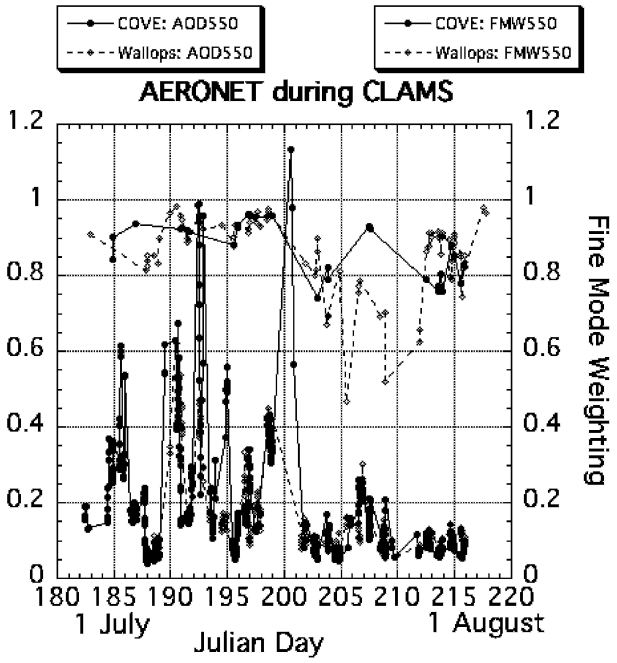

FIG. 2. Time series of AERONET-measured aerosol optical depth and fine-mode weighting at 0.55 μm during CLAMS. Two sites, COVE and Wallops, are plotted. Day 182 is 1 Jul, and day 213 is 1 Aug.

channels would also be of like consistency and quality. Therefore, we combined all sun-photometer data into one big dataset for MODIS comparison. We employed the spatial–temporal approach of Ichoku et al. (2002a), comparing averaged sun-photometer aerosol properties over 1 h (± 30 min of MODIS overpass) with averaged MODIS aerosol retrievals over a 50 km × 50 km box around the sun-photometer site. As most CLAMS sun-photometer data were obtained near the coastline, in many cases there were both ocean and land retrievals from MODIS.

a. Aerosol optical depth

Figure 3 is a scatterplot of MODIS-ocean AOD versus sun-photometer AOD at different wavelengths and channels (represented by different colors and symbols). The black dashed lines represent the MODIS "expected error," introduced by Remer et al. (2002) to contain the mean and first standard deviation (66%) of all points (i.e., $\tau = \pm 0.03 \pm 0.05\tau$). The regression lines for all wavelengths indeed fit inside the error lines, even at the longer wavelengths. All regressed y offsets are near zero (all less than or equal to 0.03), slopes are near one (between 0.87 and 1.05), and the correlation coefficients (R^2) are all greater than 0.5. In fact, for the shorter wavelengths (0.47 through 0.87 μm), correlation coefficients were greater than 0.9. At 2.1 μm, the regression is near perfect, but it should be noted there are only five points.

The regression results mean that biases are minimal for the CLAMS region during July–August 2001 and that this dataset is large enough (spatially and temporally) to provide statistical robustness, suitable for climate applications. Regression lines and monthlong statistics do not tell the whole story, however. Accuracy of individual retrievals also must be examined. During CLAMS, 86% of all individual ocean retrievals at 0.55 μm lie within the expected error lines. At least 66% of individual retrievals fall within the error bars at all wavelengths. For every case of AOD > 0.15 (at any wavelength), MODIS retrieves within the error bars. For lower AOD, where presumably noise (e.g., ocean reflectance) may be relatively larger, the MODIS AODs are symmetric around the one-to-one line, contributing insignificant bias. These results during CLAMS suggest that the MODIS aerosol algorithm is performing within published expectations, even at the longer wavelengths.

Over land, the MODIS spectral AOD is definitely not as accurate as over ocean. Figure 4 plots AOD comparisons over land. This time the expected error bars (dotted black lines) are from the Remer et al. (2005) validation over land, (i.e., $\tau = \pm 0.05 \pm 0.15\tau$). The correlation is disappointing, and a majority of MODIS retrievals are outside the expected error. Generally MODIS overestimates AOD for low aerosol loadings and underestimates for higher AOD. In the blue (0.47 μm) channel, the offsets are larger than in the red (0.66 μm) channel (0.26 versus 0.17), but the slopes are closer to one (0.76 versus 0.46). Correlation is larger in the blue ($R^2 = 0.5$) than in the red ($R^2 = 0.17$). In the green channel, all regression parameters are between the blue and red values.

Because MODIS uses different algorithms over land and ocean, it should not be expected that MODIS would retrieve identical AODs. However, we expected that the retrieved aerosol properties should at least be similar. Figure 5 shows AOD comparisons for

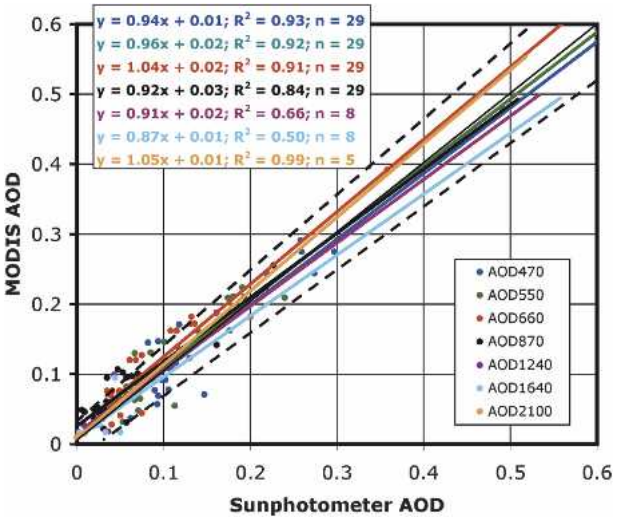

FIG. 3. Scatterplot of MODIS vs sun-photometer aerosol optical depth over the ocean during CLAMS for the seven MODIS ocean wavelengths. The MODIS-expected error is denoted by the black dashed lines. Note that many points are hidden by the regression lines.

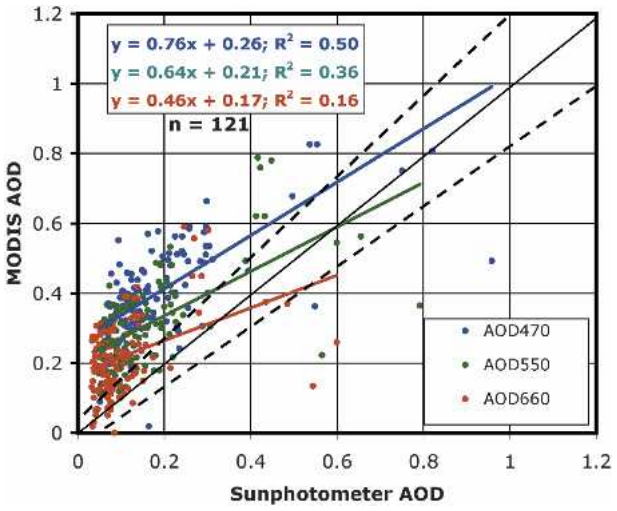

FIG. 4. Scatterplot of MODIS vs sun-photometer aerosol optical depth over the land during CLAMS for the three MODIS land wavelengths. The MODIS expected error is denoted by the black dashed lines.

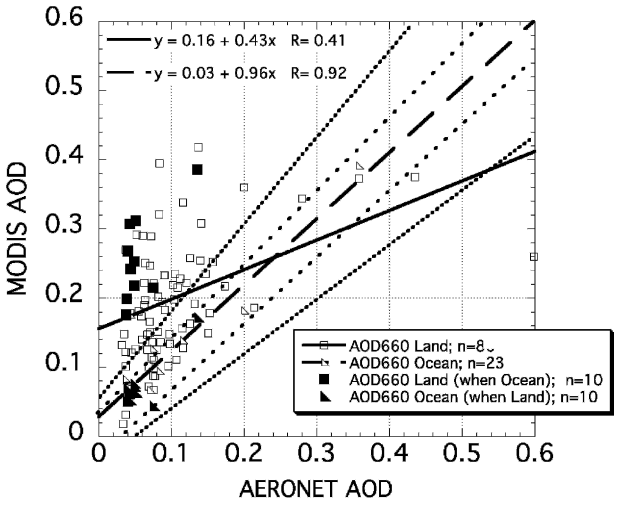

FIG. 5. Comparison of land and ocean AOD retrievals from MODIS referenced to AERONET. The open symbols represent ocean and land retrievals separately, whereas the filled symbols represent simultaneous ocean and land retrievals. The sparse and concentrated dotted lines are the MODIS-expected errors for ocean and land, respectively.

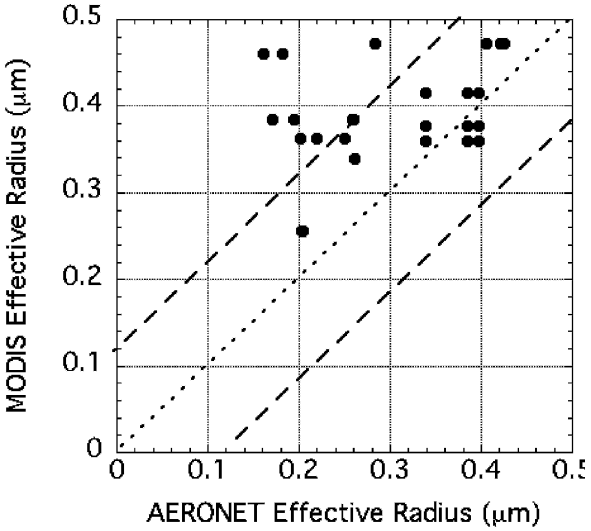

FIG. 6. Effective radius retrievals from MODIS over ocean vs AERONET. The dashed lines are ±0.11 μm, and the dotted line is the 1:1 line.

AERONET only, both over ocean and over land. The black symbols represent ocean and land retrievals separately, while the red shapes display AOD retrievals when both ocean and land retrievals were made. In all cases, the retrieved land values were much larger (often more than double) the ocean values.

b. Aerosol effective radius over ocean

Over the ocean, MODIS–sun photometer correlations at all wavelengths imply that the spectral dependence of the AOD was successfully retrieved. Assuming correct model assumptions, retrievals of aerosol size parameters should also have been good. The effective radius is defined in appendix B.

Figure 6 is a scatterplot comparing the MODIS effective radius (over the ocean only) with a similar quantity retrieved from AERONET (the other sun photometers do not retrieve size information). It is clear that MODIS generally overestimates effective radius over ocean. This means that while the spectral dependence of the MODIS retrieval is accurate to within specified uncertainties, the aerosol size model assumptions may not be. Note that MODIS sensitivity to aerosol size is reduced at low aerosol signal. During CLAMS, AOD at 0.55 μm was less than 0.15 in all but two ocean validation points. We compare the MODIS and AERONET size distributions in the next section.

c. Aerosol size distributions

A quantity, called the fine-mode weighting, is retrieved by both AERONET and MODIS. The definitions, however, are different. AERONET estimates the fraction of the total volume distribution contributed by fine aerosol (defined all aerosol of radius less than 0.6 μm). MODIS over land makes a qualitative estimate of the fraction of the total aerosol contributed by the fine model (e.g., fraction of urban/industrial aerosol to the total aerosol). Note that the "model" is a combination of multiple lognormal "modes." MODIS over ocean estimates the fraction of the total optical depth contributed by the fine (lognormal) mode. [See Remer et al. (2005) for additional explanation]. The definitions for FMW are sufficiently different so that comparison between the two is not appropriate. Nonetheless, we desire to compare retrieved size distributions from AERONET to MODIS over land and MODIS over ocean, separately. We must derive size distributions that are relative to the same scale.

The MODIS over-ocean algorithm retrieves three pieces of information (Tanré et al. 1996). These include the total AOD, the chosen fine and coarse modes, and the FMW. Using the chosen modes and the fine-mode ratio, we can go backward to infer the relative aerosol size distribution. The modes are "optical" modes, and there is no direct conversion to size distribution units (such as $\mu m^3\ \mu m^{-2}$). Thus we chose to keep the unitless size distributions and concentrate on the relative maxima and standard deviation of the size modes during CLAMS.

Using results from already produced spatiotemporal MODIS–AERONET comparisons (Ichoku et al. 2002a), we were able to recreate 10 km × 10 km aerosol products. Weighting each retrieval appropriately, we determined the aerosol size distribution that represented the 50 km × 50 km box, using the formula:

$$\frac{dV(r)}{d\ln r} = \sum_{i=1}^{i=\#\text{ pixels}} \frac{1}{\sigma_{i,\text{fine}}\sqrt{2\pi}} \exp\frac{-[\ln(r/r_{v_{i,\text{fine}}})]^2}{2\sigma_{i,\text{fine}}{}^2} + \sum_{i=1}^{i=\#\text{ pixels}} \frac{1}{\sigma_{i,\text{course}}\sqrt{2\pi}} \exp\frac{-[\ln(r/r_{v,i,\text{coarse}})]^2}{2\sigma_{i,\text{coarse}}{}^2}, \quad (1)$$

thus obtaining the unitless aerosol volume per atmospheric cross section for a log-radius bin $dV(r)/d\ln r$. In the equation, $r_{v'i,\text{mode}}$ and $\sigma_{i,\text{mode}}$ are the modal mean and standard deviation (or spread) of the retrieved aerosol mode indices for each MODIS retrieval pixel. We then averaged the curves for all 50 km × 50 km boxes to obtain the MODIS-derived unitless aerosol size distribution from CLAMS. The total unitless aerosol volume was set at 5.

Appropriate for the CLAMS location and season, the MODIS land algorithm combined the Remer and Kaufman (1998) urban/industrial aerosol model (hereby known as the RK model) with the over-land dust model (Kaufman et al. 1997b; Remer et al. 2005). To fairly compare the over-land relative modal maxima and standard deviation with those derived over ocean, we needed to derive normalized, unitless over-land size distributions, also having a total unitless "volume" of 5. This quantity was obtained using an equation similar to Eq. (3), but substituting the physical aerosol volume V_0 for 1 in the numerator. The volume per log-radius bin, $dV(r)/d\ln r$, looks like

$$\frac{dV(r)}{d\ln r} = \eta \sum_{i=1}^{i=\#\text{ modes}} \frac{V_{0,j}(r)}{\sigma_{i,\text{urban}}\sqrt{2\pi}} \exp\frac{-[\ln(r/r_{v_{i,\text{urban}}})]^2}{2\sigma_{i,\text{urban}}{}^2} + (1\text{-}\eta) \sum_{i=1}^{i=\#\text{ modes}} \frac{V_{0,i(r)}}{\sigma_{i,\text{dust}}\sqrt{2\pi}} \exp\frac{-[\ln(r/r_{v_{i,\text{dust}}})]^2}{2\sigma_{i,\text{dust}}{}^2}, \quad (2)$$

where η is the FMW (fraction of RK model to the total).

During CLAMS, size distributions from AERONET almucanturs were retrieved using the method of Dubovik and King (2000). These are physical volume size distributions (units of $\mu m^3\ \mu m^{-2}$) retrieved independently within 22 equal log-radius size bin intervals between 0.05 and 15 μm. Again, like the MODIS over-land size distributions, we made the AERONET retrievals unitless, by setting the total aerosol volume equal to 5.

Figure 7 visually shows CLAMS-averaged aerosol size distributions independently retrieved by the over-ocean (blue curve) and over-land (green curve) algorithms from MODIS, and from AERONET almucantar radiance inversions (red curve). Clearly, the size distributions are not the same. Although all three have fine-mode peaks at approximately 0.15 μm, the AERONET fine-mode peak has much smaller width or standard deviation. The contribution to the total volume is larger for ocean than for land near the inflection point (fine/coarse-mode split at 0.6 μm), but smaller as the radius increases over 1 μm. Because the AERONET retrievals are split into fine and coarse mode at a radius of 0.6 μm, radii bins near 0.6 μm are not well represented.

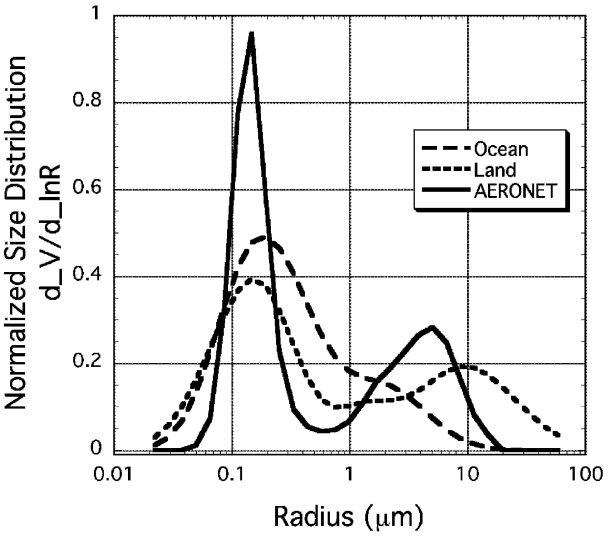

FIG. 7. CLAMS-averaged "equal total volume" aerosol volume distribution from MODIS over ocean and land, and from AERONET inversions.

The scattering effects of aerosols in the CLAMS size range are best explained by estimating surface area distributions. Figure 8 is analogous to Fig. 7, but plots surface area distribution, such that each area distribution curve encloses the same total aerosol unitless surface area. For CLAMS, the aerosol fine mode clearly dominated the area size distribution, presumably domi-

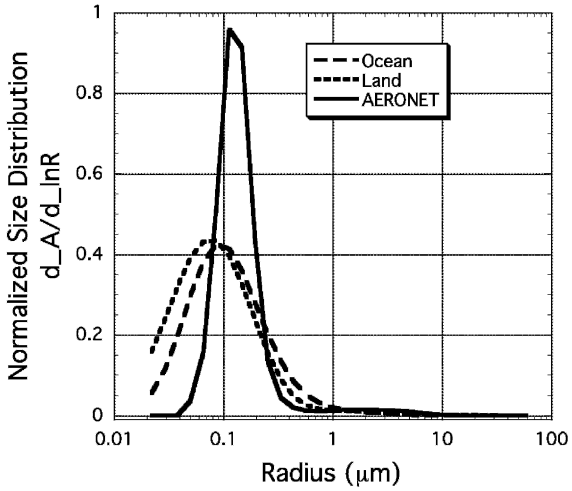

FIG. 8. CLAMS-averaged "equal total surface area" aerosol surface area distribution from MODIS over ocean and land, and from AERONET inversions.

nating aerosol scattering. There is, however, a small contribution from the coarse mode (just above 0.6 μm), especially as retrieved by the ocean retrieval.

One easy way to compare the size distributions is to compute the modal radius r_v, standard deviation of the modal radius σ, and the effective radius r_{eff}. We used the strategy prescribed by AERONET (splitting at 0.6 μm) to define fine and coarse mode. The definition for each parameter is found in appendix B.

Table 2 shows the calculations for average CLAMS effective radii, modal radii, and standard deviation. The AERONET and ocean fine-mode effective radii are nearly the same, with the land values being smaller. On the other hand, the coarse mode for land better agrees with AERONET. For the total effective radius, all three values are close, and in the end land and ocean retrievals are nearly exact. AERONET retrieves slightly larger total effective radius. The largest differences between MODIS size retrievals and those from AERONET are the fine-mode standard deviation, σ_f.

5. Land retrieval discussion

From Fig. 4, we see that the MODIS–sun photometer AOD correlation line has both a significant positive offset and a slope less than one. The *y* offset (MODIS retrieves AOD when in fact there is none) implies errors induced by assuming inappropriate surface reflectance. On the other hand, the less-than-one slope implies errors in the aerosol models. In the following two sections, we address each of these problems and introduce reasonable solutions that may be used in future MODIS code updates.

a. Aerosol model updates and correcting the slope

Ichoku et al. (2003) showed that MODIS retrieval errors for fresh smoke during the Southern African Regional Science Initiative (SAFARI-2000) could be significantly reduced by simply decreasing the single scattering albedo of the African smoke model. There is little evidence in the literature that the current single scattering albedo for the RK model (0.96) may be wrong; therefore we must find another way to correct the less-than-one slope in Fig. 4.

TABLE 2. CLAMS-averaged total, coarse-mode, and fine-mode modal radius, standard deviation τ, and effective radius r_{eff} calculated from MODIS over ocean, over land, and by AERONET.

Mode	$r_v(\mu\text{m})$	τ	r_{eff}
Ocean			
Fine	0.178	0.718	0.136
Coarse	1.870	0.724	1.498
Total	0.327	1.258	0.178
Land			
Fine	0.143	0.746	0.108
Coarse	6.166	1.137	3.334
Total	0.708	2.081	0.183
AERONET			
Fine	0.149	0.410	0.138
Coarse	3.657	0.696	2.849
Total	0.493	1.638	0.214

1) URBAN/INDUSTRIAL AEROSOL MODELS

The dynamical urban/industrial aerosol model, currently used in the MODIS algorithm over land (Kaufman et al. 1997b), was described fully in Remer and Kaufman (1998). The optical properties of the RK-model, shown in Table 3, were derived from data collected during the Sulfates, Clouds and Radiation—Atlantic (SCAR-A) experiment. During SCAR-A, Cimel sun photometers were operated at five locations along the U.S. East Coast, between July and September 1993, where and when hazy/polluted conditions are commonly observed. After cloud screening and almucantur symmetry determination, the method of Nakajima et al. (1996) was used to retrieve aerosol size volume distributions from 125 sky radiance measurements. These aerosol volume distributions were then binned and averaged by optical depth, yielding a dynamical dependence on the AOD. Remer and Kaufman (1998) noted that the AOD dependence explained 60% of the variance in the shift (growth) of the aerosol modes and the total volume distribution. Figure 9 shows some calculations of the volume distribution for selected optical depths at 0.44 μm, where a realistic Ångström exponent of 1.8 was used to extrapolate AOD from 0.67 to 0.44 μm. This extrapolation was necessary because the RK model is defined at 0.67 μm and was done in order to easily compare to the new model, described next.

A new dynamical urban/industrial aerosol model was developed using 8 yr of AERONET data from NASA Goddard Space Flight Center (GSFC) and is described in detail in Dubovik et al. (2002). This is referred to here as the D model. To derive this model, spectral AOD and almucantar sky radiance were inverted by the method of Dubovik and King (2000) to retrieve aerosol size distributions and aerosol optical properties. Measurements were made both leftward and rightward from the sun, and only radiances that were suitably symmetric were used. The retrievals were further constrained by performing inversions at large azimuth angles from the sun. In most cases, the theoretical radiances were matched with observed radiances with errors less than 5%. Like the RK model, the D model's size distribution is a dynamical function of the AOD, valid when the AOD at 0.44 μm is at least 0.05. Unlike the RK model, a trimodal distribution, the D model is a bimodal lognormal distribution. Particles with radius less than 0.6 μm belong to the fine mode, and those larger than 0.6 μm belong to the coarse mode. Table 4 lists the D model size and optical parameters for urban/industrial aerosol. Figure 10, like Fig. 9, shows size distribution as a function of the AOD at 0.44 μm. Note that in this case, the size distribution is defined at 0.44 μm, so no extrapolation was necessary.

TABLE 3. Model parameters and standard deviation for MODIS urban/industrial model over land. Volume (V_0) is volume per atmospheric cross section in units of μm, which is equivalent to 10^{-4} cm^3 cm^{-2}; τ_{670} is the AOD at 0.67 μm. Adapted from Remer and Kaufman (1998; their Table 1).

Mode	$r_g(\mu m)$	$r_v(\mu m)$	τ	$V_0(\mu m)$
acc-1	0.036	0.11 ± .01	0.60 ± 0.11	$-0.015 + 0.51\tau_{670} - 1.46\tau_{670}^2 + 1.07\tau_{670}^3$
acc-2	0.11	0.21 ± 0.025	0.45 ± 0.07	$0.0038 - 0.086\tau_{670} + 0.90\tau_{670}^2 - 0.71\tau_{670}$
Salt	0.99	1.30 ± 0.10	0.30 ± 0.10	$-0.0012 + 0.031\tau_{670}$
Coarse	0.67	9.50 ± 4.0	0.94 ± 0.20	0.045 ± 0.028

There are substantial differences between the D model and the RK model. The fine mode for the D model has a peak at a slightly smaller radius, with narrower curvature (smaller σ). The coarse-mode RK model's (centered around 9 μm) lack of AOD dependence looks unphysical, but the D model's is more realistic and better defined. The refractive indices (m) differ as well. The RK model uses $m = 1.43 + 0.0035i$ for the accumulation modes, $1.43 + 0.0i$ for the marine (salt) mode, and $1.53 + 0.008i$ for the coarse (dust) mode. For both fine and coarse modes, the D model's refractive index is a function of AOD, that is, $m = 1.41–0.03\tau_{440} + 0.003i$, where τ_{440} is the AOD at 0.44 μm. For the AOD ranges in Figs. 9 and 10, this means the real part m ranges between about 1.41 and 1.38, which is closer to that of water (m_r=1.33) than used in the RK model.

2) CONVERSION TO THE DUBOVIK ET AL. URBAN/INDUSTRIAL MODEL

Here, we attempted to "correct" the less-than-one slope seen in Fig. 4 by replacing the operational RK model by the newer D model. We created two lookup tables, one for each aerosol model. Using a single value of solar/surface/satellite geometry and spectral surface albedo for both tables, we ran the Second Simulation of the Satellite Signal in the Solar Spectrum (6S) radiative transfer code (Vermote et al. 1997b) to simulate apparent (satellite) reflectance as a function of AOD. Figure 11 plots apparent reflectance in three MODIS wavelengths (0.47, 0.66, and 2.1 μm) for one example of a solar/surface/satellite geometry, commonly observed during CLAMS. As in section 5a(1), we assumed a realistic Ångström exponent of 1.8 to interpolate between wavelengths.

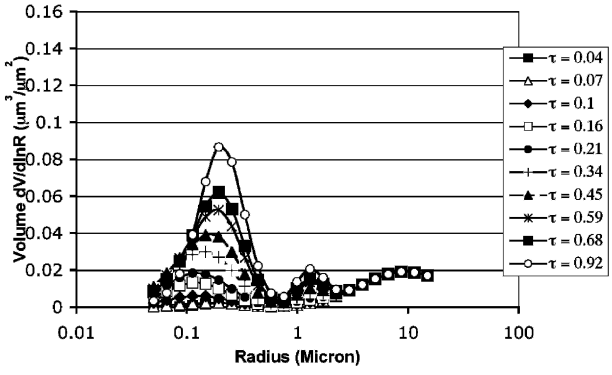

FIG. 9. Volume size distribution for the dynamic urban/industrial aerosol models of Remer and Kaufman (1998). Curves are functions of optical depth at 0.44 μm (τ).

Conversion from one aerosol model to another is also illustrated in Fig. 11. Following a line of constant apparent reflectance ($\rho = 0.16$ in the example), we can graphically derive the AOD under both models. In this example, an RK model AOD of 0.5 produces the same apparent reflectance in the blue as a D model AOD of 0.7. The same exercise was done at all three land wavelengths. In essence, we created a transformation from RK model "space" to D model "space."

Figure 12 shows how swapping models could apply to the CLAMS data. The red and blue solid lines replot the regression lines from Fig. 4. Assuming that all geometry behaves like the example shown in Fig. 11, conversion from the RK model to the D model results in the red and blue dashed lines. The slopes for the dashed lines are increased (from 0.76 to 1.23 in the blue and from 0.46 to 0.58 in the red). The offsets are unchanged, because of the same reflectance for both models at zero AOD. This suggests that the D model may be better than the RK model for the CLAMS data. Note, however, that our assumption of a single geometry for all CLAMS is questionable, and inclusion of angle dependence could have changed the plot drastically. This exercise, nonetheless, demonstrates that the retrieval is sensitive to the assumed aerosol models, and that updating aerosol models can improve the products.

b. Surface reflectance assumptions and correcting the offset

Both measurements (Kaufman and Remer 1994; Kaufman et al. 1997c) and theoretical studies (Kauf-

TABLE 4. Summary of aerosol optical properties retrieved from 2400 GSFC AERONET measurements., where (V_0) is volume per atmospheric cross section in units of μm^3 μm^{-2} (or μm) and τ_{440} is the AOD at 0.44 μm. Adapted from Dubovik et al. (2002; their Table 1).

Mode	$r_v(\mu m)$	τ	$V_0(\mu m)$
Fine	$0.12 \pm 0.011\tau_{440}$	0.38 ± 0.01	$0.15(\tau_{440})\pm0.03$
Coarse	$3.03 \pm 0.049\tau_{440}$	0.75 ± 0.03	$0.001 + 0.04(\tau_{440})\pm0.01$

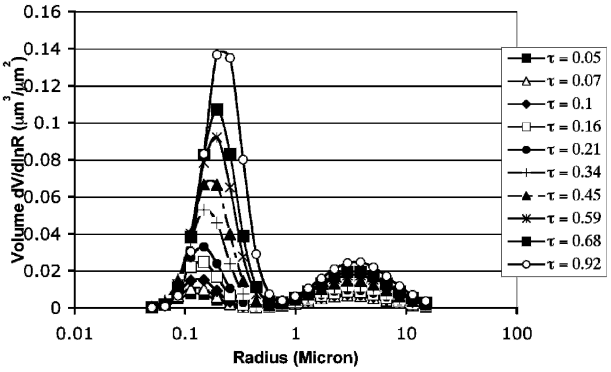

FIG. 10. Volume size distribution for the dynamic urban/industrial aerosol model of Dubovik et al. (2002). Curves are functions of optical depth at 0.44 μm (τ).

man et al. 2002) have demonstrated a relationship between visible and IR surface reflectance ρ_λ, for certain vegetated surfaces throughout the globe. Generally it was shown that $\rho_{0.47} \approx 0.25\rho_{2.1}$ and $\rho_{0.66} \approx 0.5\rho_{2.1}$, which are both assumed equalities by the operational MODIS retrieval over land (Kaufman et al. 1997b). We refer to $\rho_{0.47}/\rho_{2.1}$ and $\rho_{0.66}/\rho_{2.1}$ as the blue/IR and red/IR ratios, respectively, and collectively as the VIS/IR ratios.

These relationships do not hold for specific regions, including the U.S. East Coast. Remer et al. (2001) measured surface reflectance aboard a low-flying aircraft and found that the VIS/IR ratios depend on geometry. Generally, the red/IR ratio is less than 0.5 for backscattering view angles and is greater than 0.5 for forward scattering. They also found seasonal differences that were weakly correlated with changes in the "greenness" of the surface (such as might be associated with the NDVI). The blue channel (0.47 μm) exhibited similar deviations from assumed ratios when viewed from the aircraft.

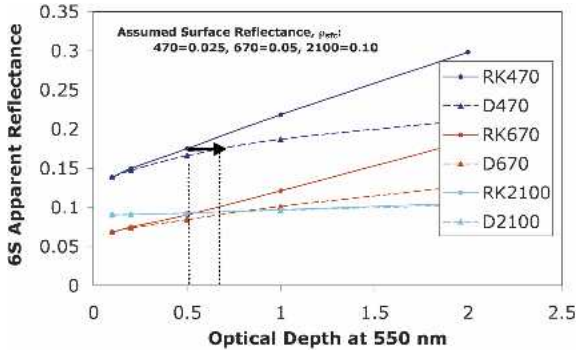

FIG. 11. Conversion from the RK model (labeled "R") to the D model (labeled "D"). Apparent (satellite) reflectance has been calculated using 6S code. Black arrow shows conversion for a given apparent reflectance. The solar zenith angle is 30°, the solar azimuth angle is 120°, the satellite view zenith angle is 45°, and the satellite view azimuth angle is 95°.

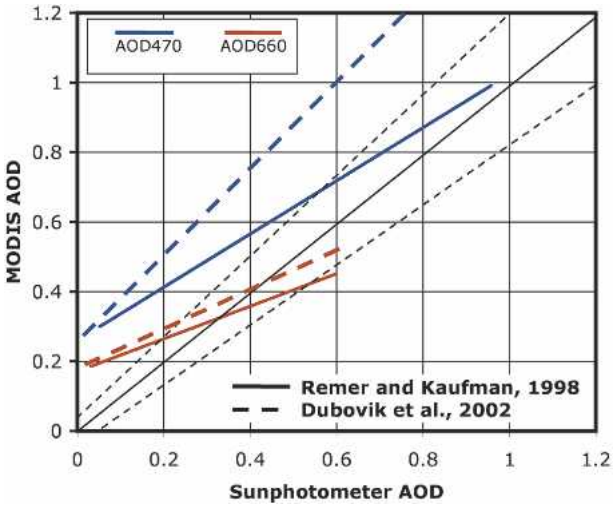

FIG. 12. Empirically corrected optical depths over land. Solid red and blue lines are the regression lines from Fig. 4. The red and blue dashed lines are the corrected optical depths. The black lines are the expected errors from Fig. 4.

The landscape along the U.S. East Coast is very heterogeneous, containing urban areas, forests, and grassy/agricultural fields. Because of ample rainfall and proximity to the ocean, small land water bodies (such as puddles or swamps) are also ubiquitous and may be underneath the tree canopy. While the MODIS over-land algorithm attempts to mask even the most shallow water bodies, puddles and swamps are not always completely masked out. Because water is nearly black (zero reflectance) in the mid-IR (2.1 μm), assuming the standard VIS/IR ratios would result in overestimating the aerosol path reflectance, mirroring the y offsets seen in Fig. 4. Some of the outlying very high VIS/IR points displayed in Remer et al. (2001) were indeed measured over swamps or puddles in forests.

ATMOSPHERIC CORRECTION OF CLAMS DATA

What were the actual surface reflectance ratios during CLAMS? One strategy is to assume that clean aerosol conditions lead to surface reflectance retrievals with small atmospheric contamination. Operational MODIS surface land products (Vermote et al. 1997a) employ this strategy to provide land reflectance products from MODIS by searching for the cleanest cases in 8- or 16-day periods, and assuming appropriately low AOD. Because we have measured spectral AOD from sun photometers during CLAMS, we can do even better. We know the spectral optical conditions exactly.

Atmospheric correction is the process of determining the surface reflectance that would be measured if there were no atmosphere (Kaufman et al. 1997a). Vermote et al. (1997a) describes how the atmospheric correction could be applied to MODIS over land. Using the

MODIS level 1B radiance data as the primary input, the satellite reflectance is corrected for Rayleigh scattering, aerosol scattering, and coupling between the atmospheric and surface reflectance functions. The 6S code includes a module for performing atmospheric correction with MODIS data (Vermote et al. 1997b), which includes trace gas and ozone assumptions.

On 1 August, the AERONET instruments at both Wallops and Oyster reported very clean (low AOD) and dry (relative to normal summertime) atmospheric conditions. The AOD at 0.44 and 0.67 μm were 0.11 and 0.05, respectively, whereas the column precipitable water vapor (PW) was 2.4 cm. Assuming the U.S. standard (COESA 1976) midlatitude profile for temperature, ozone gas climatology, and near-zero AOD at 2.1 μm, 6S was used to provide atmospheric corrected reflectance over much of the local CLAMS region (small box in Fig. 13). Figures 14a, 14b, and 14c show the resulting atmospherically corrected surface reflectance at 0.47, 0.66, and 2.1 μm respectively, on a 500-m resolution. Figures 15a and 15b show the resulting blue/IR and red/IR reflectance ratios over the same region. Note the bright clouds in Fig. 13 that carry over to Fig. 14 as high reflectances and to Figs. 15a and 15b as high ratios. These clouds would be masked by the standard MODIS algorithm.

Over much of the grassy and agricultural regions (central peninsula), the reflectance ratios are generally lower than the assumed ratios, about 0.13 for red/IR and 0.45 for blue/IR. Toward the coastline, however, sandy beach shores (bright in the visible) alternate with swampy forests (very dark at 2.1 μm), increasing the VIS/IR ratios. Here, the ratios can be much, much higher, approaching 0.7 for the blue/IR and 0.8 for the red/IR. These ratios, much higher than the assumed values, could introduce significant offsets into the retrieved AOD values. The operational algorithm should be selective in the pixels it keeps for retrieval, mitigating these effects. The possibility, however, exists for the type of significant offsets we see in the scatterplots.

After using the operational algorithm to degrade the 500-m pixels into 10 km (cloud masking, sorting and removing the darkest and brightest pixels), we then applied atmospheric correction (with the AERONET data as input). The resulting reflectance ratios in a 10-km box were still quite high. Over Wallops, for example, the atmospherically corrected reflectance ratios over land were about 0.4 and 0.6 for blue/IR and red/IR, respectively. At Oyster, these ratios were closer to 0.5 and 0.7. Further degradation to a 50 km $\times$ 50 km box (for the spatiotemporal validation) over the area resulted in ratios of about 0.45 and 0.63. This strong discrepancy between derived ratios and assumed ratios is likely a major source for the y offsets, especially in the blue, where the discrepancy is largest.

For the 1 August CLAMS case, we performed the

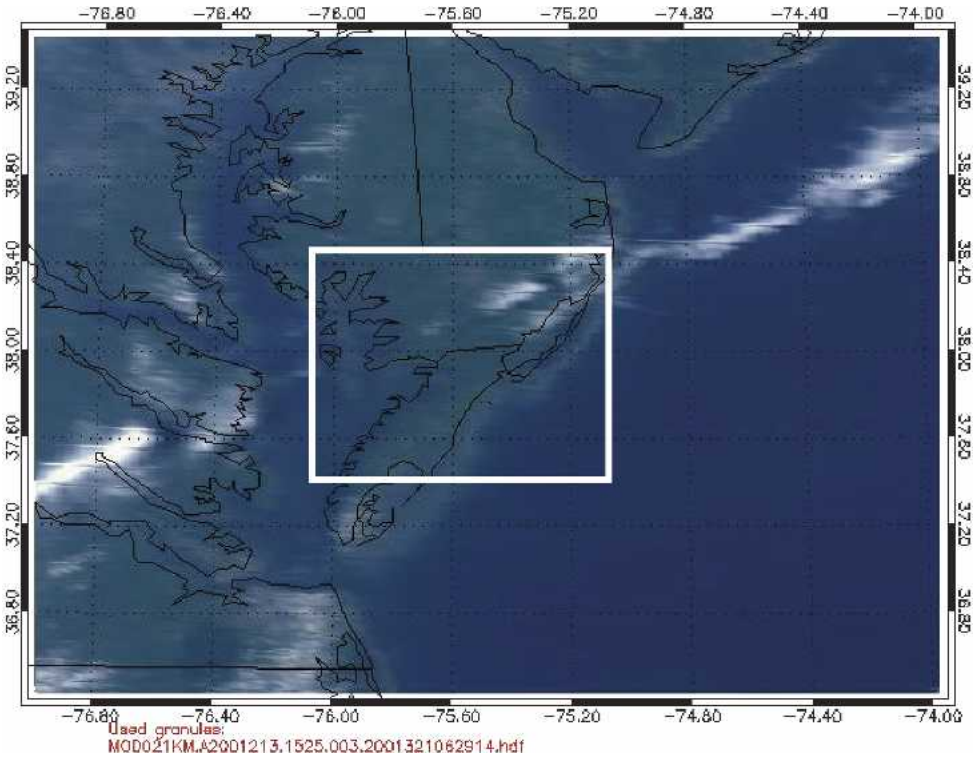

FIG. 13. Red–green–blue (RGB) visible image of MODIS granule used in atmospheric correction exercise (1 Aug 2001). The white box approximates the area that is analyzed.

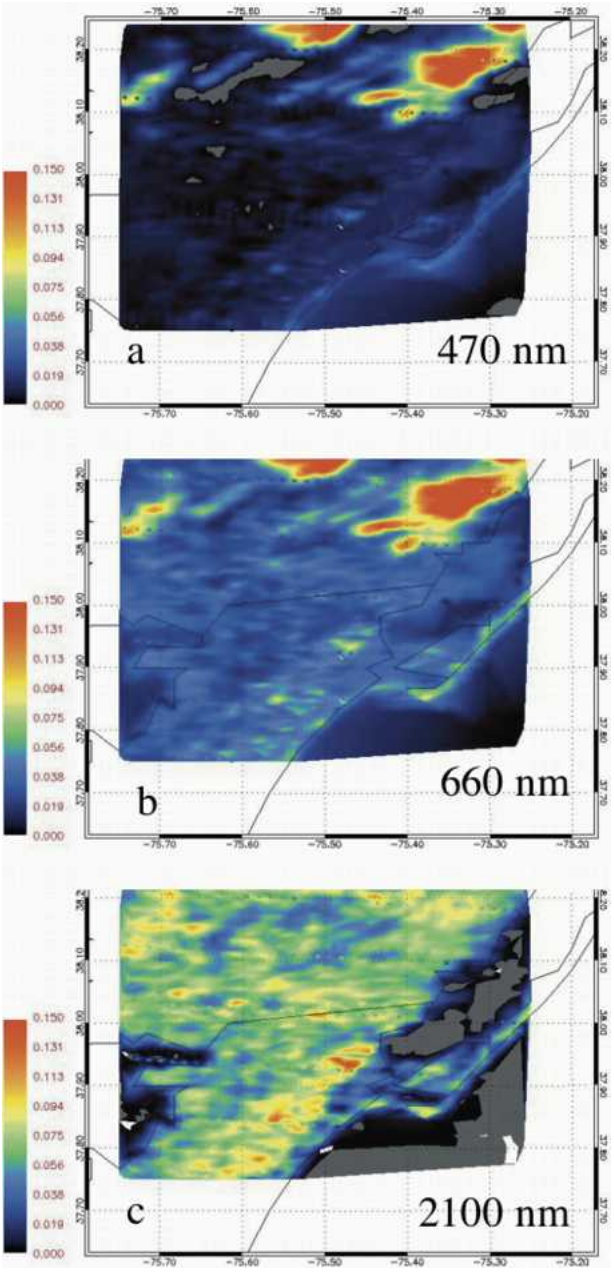

FIG. 14. (a) Atmospherically corrected surface reflectance at 0.47 μm for a small portion of the 1 Aug 2001 granule shown in Fig. 13. The bright reflectance in the upper portion of the image corresponds to the white clouds seen in Fig. 13. (b) Same as for Fig. 14a, but for 0.66 μm. (c) Same as for Fig. 14a, but for 2.1 μm. The clouds in the upper portion of the image seen in Fig. 13 are not as distinct at 2.1 μm.

operational MODIS retrieval (applying the RK model), but replaced the assumed blue/IR and red/IR surface ratios (0.25 and 0.5) by the derived ratios (0.45 and 0.63). In Fig. 16, we display images of both (a) the operational AOD retrieval and (b) the new AOD retrieval using the derived ratios. Clearly, the use of the derived ratios removes much of the AOD discontinuity over the coastline. However, some of the pixels far from the coastline were removed, where presumably the derived ratios caused the algorithm to overcorrect for the surface and retrieve AOD below zero. This implies that these new ratios are not global in nature.

The AERONET sites in the CLAMS region are concentrated near the coastline, so that MODIS–AERONET *y* offsets should be improved by the use of the more appropriate regional surface reflectance ratios. Figure 17 compares AODs from MODIS and coastal AERONET sites, for MODIS AOD derived using old and new (derived) surface reflectance ratios. This plot used as inputs only data where the AOD in the red was less or equal to 0.25, in order to more clearly show the improvement in offset. The RK model for urban/industrial aerosol is used in both runs, thus comparing only the introduction of new ratios. As all AERONET sites plotted here were located near the coastline, introduction of the new surface ratios deleted only 1 point (out of 41) from the set of old ratio data. At least along the coastline, we see that application of the new ratios substantially lowered the *y* offsets, thus providing improvement to spectral AOD retrievals.

6. Conclusions

Comparisons have been made between MODIS data and sun-photometer data during the CLAMS experiment of July–August 2001. The sun-photometer measurements included data from AERONET Cimels, handheld Microtops II, Langley, and AATS-14 sun photometers. These sun-photometer datasets were among the first to include longer IR wavelengths (1.6 and 2.1 μm) that were directly or nearly directly comparable with the MODIS longer wavelengths. After later corrections of the Microtops II data for temperature, water vapor, and CO_2, all four datasets were calibrated to similar accuracies.

Aerosol optical depths over the ocean retrieved from MODIS compared well to AODs measured by the sun photometers, even at the longer IR wavelengths. All regression lines fell within published error bars (Remer et al. 2005), offsets were near zero, slopes were near one, and correlation was greater than 0.5 ($>$0.9 for 0.47 through 0.87μm). At 2.1 μm, the regression was near perfect, but there were only five points. For all wavelengths, at least two-thirds of the individual retrievals were contained within the error bars, including 86% at 0.55 μm. Sixty-six percent of MODIS effective radii were within $\pm$0.11 μm of AERONET derived values; the remaining points were overestimated by MODIS. These results suggested that the MODIS algorithm over ocean was performing at least as well as published expectations.

Over the land, however, MODIS generally performed below expectation. AODs were overestimated

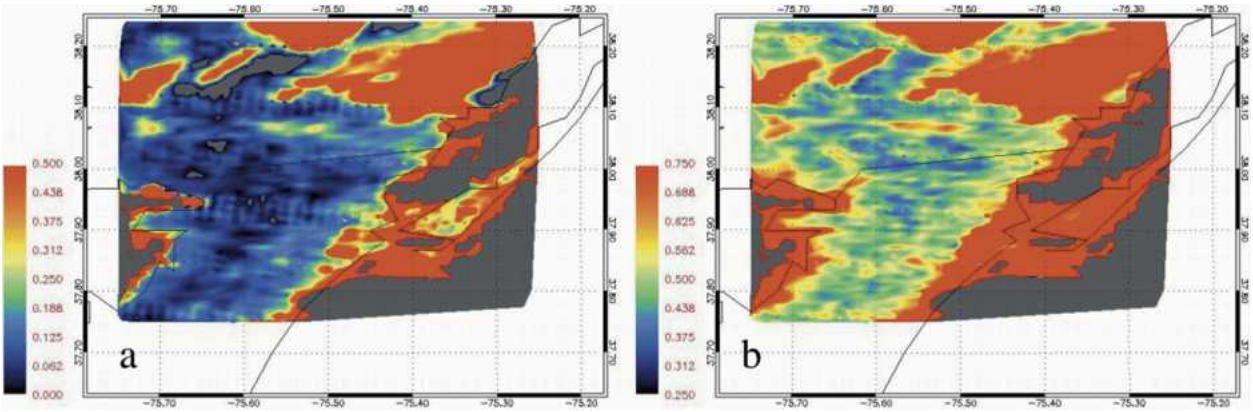

FIG. 15. (a) Surface reflectance ratio 0.47 μm /2.1 μm for atmospherically corrected 1 Aug 2001 granule shown in Fig. 13. The high ratios in the upper portion of the image are due to clouds that would ordinarily by masked out by the operational algorithm. (b) Same as for Fig. 15a, but for 0.66 μm /2.1 μm ratio.

for low aerosol loadings and underestimated for higher loadings. In the blue, the offsets were larger than in the red, but the slopes were closer to one. Correlation was larger in the blue ($R^2 = 0.5$) than in the red ($R^2 = 0.17$). All regression parameters derived for the interpolated green channel fit between the values for blue and red channels.

Because of differing definitions, the MODIS fine-mode weighting products retrieved from both land and ocean algorithms separately were not easily compared with AERONET retrievals from sky radiance measurements. Instead we derived averaged normalized (unitless) aerosol size distributions for both ocean and land during CLAMS. These MODIS size distributions could be compared directly with similar unitless averaged AERONET size distributions. The fine-mode peaks were found at the nearly same radius in all three cases. However, the spread of the distributions was large. In the coarse mode, there was little similarity between the size distributions, but the coarse mode is known to have little influence on the visible AOD. These size distribution differences should be examined for development of future MODIS algorithms.

The MODIS-retrieved AODs over land may be improved by using a newer urban/industrial aerosol model and correcting the surface reflectance assumptions. Us-

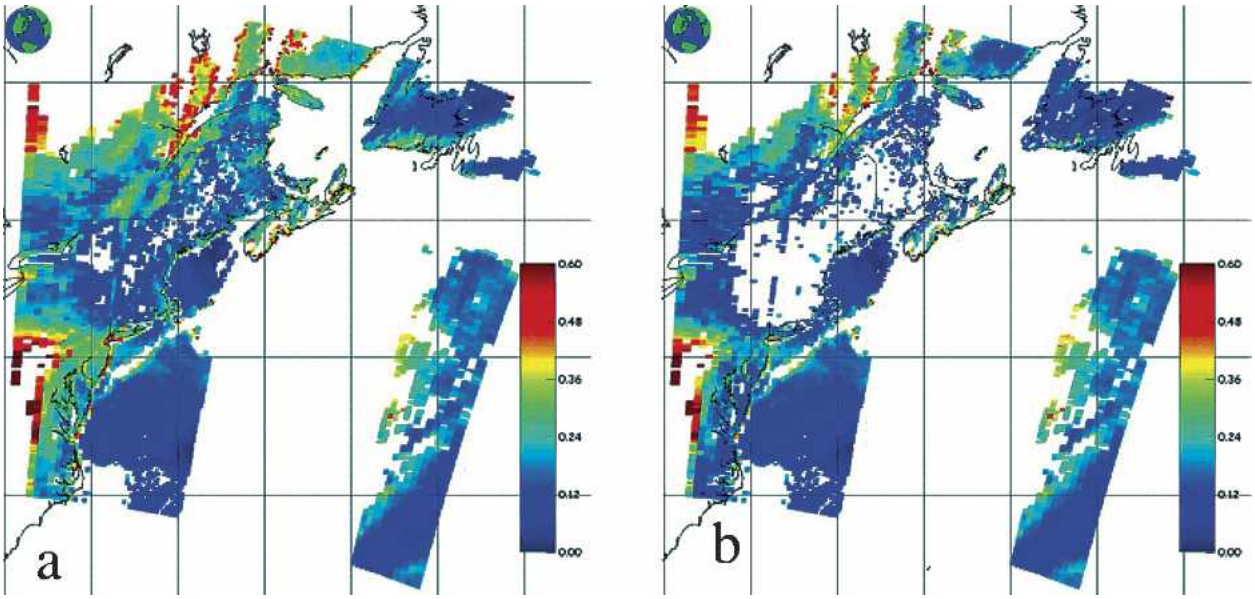

FIG. 16. (a) AOD at 0.55 μm for the 1 Aug case retrieved using the assumed VIS/IR surface reflectance ratios in the operational MODIS algorithm. Note the discontinuities along the coastline. (b) AOD at 0.55 μm for the 1 Aug case retrieved using the derived VIS/IR surface reflectance ratios in the otherwise standard algorithm. The discontinuities along the coastline have been nearly removed, but some AOD retrievals in New England are now missing.

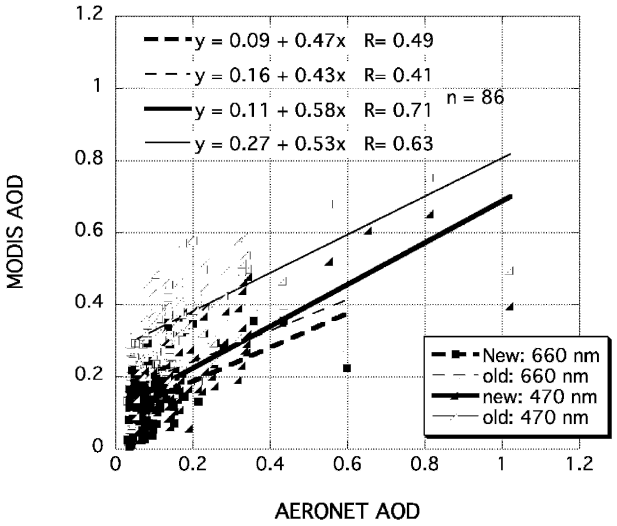

FIG. 17. Comparison of AOD retrieved by MODIS-land and by AERONET. The regular lines represent retrievals using the assumed VIS/IR surface reflectance ratios, while the bold lines represent the use of the derived surface reflectance ratios. The solid and dotted lines refer to the 0.47- and 0.66-μm channels, respectively. All points are for sun-photometer AOD at 0.66 μm less than 0.25.

ing the urban/industrial model proposed by Dubovik et al. (2002) in place of the operational Remer and Kaufman (1998) model seems to produce better sensitivity to aerosol optical depth. However, the lack of substantial statistics for moderate to large AOD prevents firm conclusions concerning the value of a change in aerosol models.

The large *y* offset seems to be the largest problem seen in the CLAMS dataset, which is likely due to inappropriate surface reflectance assumptions. Atmospheric correction of satellite radiance data, for low aerosol loadings, demonstrated that assumed VIS/IR surface reflectance ratios are not appropriate for the very dark (at 2.1 μm) surfaces observed during CLAMS. Instead, larger ratios on the order of 0.45 and 0.63 for blue/IR and red/IR, respectively, were more appropriate for CLAMS near the coastline. Further inland, the original assumed ratios seemed more appropriate. Whereas attempting derivation of global surface reflectance ratios is definitely beyond the scope of this paper, we can see how we could use atmospheric correction to derive ratios appropriate for certain regions. A new set of surface reflectance assumptions may be variable (dynamic) or collocated with a land surface product. On a regional scale, this should help to improve the MODIS aerosol product over land.

Acknowledgments. The authors thank R. Kleidman, C. Ichoku, R.-R. Li, Y. Kleidman, K. Rutledge, and the COVE staff for taking some of the Microtops measurements and J. Eilers for "tracking" the AATS-14 during CLAMS. Thanks goes to O. Dubovik and S. Mattoo for helping to understand AERONET and MODIS algorithm details. The entire AERONET staff should be commended for producing the high-quality data used in this study. Special thanks goes to K. Johnson for developing a laboratory study for providing Microtops temperature corrections, and Dr. Philippe Dubuisson (University of Littoral Côte d'Opale, France), for the line-by-line transmittance computations for the water vapor corrections. Finally, R. Dickerson should be thanked for his insight and suggestions for this paper and its hopeful start of a successful Ph.D. thesis.

APPENDIX A

Calibration of Microtops Sun Photometers

Six handheld Microtops II sun photometers were deployed during CLAMS. They are highly portable (10 cm $\times$ 20 cm $\times$ 4 cm, weighing 600 g) and are easily relocated for different measurements (Morys et al. 2001). Each instrument has five mini collimators that focus light onto five separate filters, each corresponding to one wavelength band. Using factory-prescribed electronic gains and other programmable constants (initial calibration), the instrument measures voltages induced by radiance. Given the latitude, longitude, and date/time (either entered manually or via a GPS), the pressure (measured by the instrument), the temperature (measured internally within the electronics), and the "dark current" (measured upon instrument initialization), one can convert the measured voltages into optical depths. Some assumptions about the ozone and other atmospheric absorbers are also needed for these calculations.

Two of the instruments (1 and 2; serial numbers 3761 and 3762) are "classic" Microtops II sun photometers, measuring AOD in four VIS/NIR wavelengths (centered at 0.34, 0.44, 0.675, and 0.87 μm), and columnar water vapor using 0.936 μm. The other four have been customized to include longer IR wavelengths. Two instruments (10 and 11; serial numbers 5378 and 5379), measure AOD in four wavelength bands (0.44, 0.675, 1.64, and 2.10 μm) and water vapor using 0.936 μm. The other two (12 and 13; serial numbers 5376 and 5377) measure AOD in five wavelength bands (0.38, 0.50, 0.675, 0.87, and 1.64 μm). During CLAMS, two or more instruments were operated in tandem to increase the number of wavelengths and provide intercomparison for common wavelengths.

The classic instruments were calibrated by combining Langley plots taken before CLAMS and AERONET side-by-side comparison after CLAMS. The Langley plots were performed at the solar observatory atop pristine Mauna Loa on three mornings and one afternoon during 14–17 June 2001 (just prior to CLAMS), whereas side-by-side calibration transfer was performed next to the reference AERONET Cimel at GSFC in the months after CLAMS (see Ichoku et al.

2002b). Results from these two methods yielded expected spectral AOD accuracy of ±0.03 for the classic instruments and the classic wavelengths (0.44, 0.675, and 0.87 μm) on the new instruments. However, these algorithms proved to be insufficient for calibration of the customized IR (1.6 and 2.1 μm) wavelengths. For one, AERONET does not measure in these channels, so that side-by-side calibration transfer was not possible. Also, trace gases and water vapor are important absorbers at these wavelengths. Absorption of water vapor occurs at both the 1.6- and 2.1-μm channels, while carbon dioxide and methane are absorbed at the 1.6-μm channel. Also, changes in internal instrument temperature were discovered to affect the electronic signals.

The water vapor dependence was analyzed through detailed analysis of the line-by-line water vapor absorption using the 2000 High-Resolution Transmission Molecular Absorption Database (HITRAN-2000). It was concluded that water vapor lines account for nearly 90% of the total (lines + continuum) absorption. For the U.S. midlatitude summer (US-MLS) conditions (water column of 2.9 g cm^{-2}), the water vapor contribution to the total optical depth is about 0.0045 at the 1.6-μm channel, and 0.042 at the 2.1-μm channel (±10% depending on water vapor continuum assumptions).

During CLAMS, the water vapor column (W) was usually not far off from the US-MLS value (ranging between 2 and 4 cm^{-2}), so we assumed that the water vapor optical depth was linearly proportional to the actual water column, that is,

$$\tau_w = \tau_{w\mathrm{MLS}}(W_{\mathrm{obs}}/W_{\mathrm{MLS}}),$$

where τ_w is the AOD contribution from water vapor absorption. Note that at 2.1 μm, a 0.042 water vapor optical depth is similar or greater in magnitude than an expected aerosol optical depth.

Carbon dioxide (CO_2) and methane have absorption lines near 1.6 μm (Vermote et al. 1997b). Because of the Microtops filter characteristics, these corrections are about 0.015 (A. Smirnov 2003, personal communication). This value is subtracted from all measured Microtops optical depths at this channel. Carbon dioxide and methane effects are small at 2.1 μm.

The Microtops temperature dependence on the measured signal is more complicated and is composed of both an offset (dark current/noise) and changes in the detector (or electronic gain). Temperature correction must be done separately from the original Mauna Loa calibrations, and also from the CLAMS observations. While measuring a laboratory solar simulator lamp, the Microtops was alternately heated (by an electric heating pad) and cooled (by an ice pack). Many trials were performed to retrieve voltage dependence on temperature as compared to a reference of 17°C. We found the most substantial temperature dependency in the values of dark current (offset in the calibration), although small but significant drifts were observed in the voltage values even after dark current was accounted for. These drifts were attributed to calibration gain. The relationship between voltage and temperature behaved similarly for the two channels (1.6 and 2.1 μm), but displayed different magnitudes of dependence and varied slightly between instruments.

The observations taken at Mauna Loa were corrected for these measured temperature dependencies. It was assumed that when measurements were taken more than 10 min apart, the instrument would have been turned off (either automatically or manually), so that upon reinitialization the dark current would be taken into account. Therefore, only when measurements were taken less than ten minutes apart did we correct the measured signal for dark current. The gain correction was applied across all Mauna Loa measurements.

During CLAMS, our operating procedure minimized dark current issues, because the instruments were turned off after every set of measurements. Upon initialization, new dark current measurements were taken and automatically taken into account. Only the correction for temperature-dependent gain was applied to the CLAMS data.

The processes for Mauna Loa recalibration and subsequent reprocessing of the CLAMS data were detailed. We believe that after application of all corrections, the Microtops AOD values used in this work were accurate to within ±0.03 at 1.6 μm and within ±0.04 at 2.1 μm.

APPENDIX B

Aerosol Size Parameters

The aerosol volume distribution $dV(r)/d\ln r$ is retrieved by AERONET and indirectly by MODIS. All particles smaller than 0.6 μm are considered fine, whereas those larger than 0.6 μm are coarse. Their superposition composes the total distribution. This separation of fine and coarse is seemingly arbitrary, but works in the majority of the practical cases. Each of the parameters below are defined for the (total) distribution, but by changing the limits of integration, are applicable to fine and coarse modes separately. For AERONET, the limits of integration 0 and ∞ would be replaced by 0.05 and 15.0 μm, respectively.

The aerosol volume distribution $dV(r)/d\ln r$ and surface area distribution $dA(r)/d\ln r$ are both related to the number distribution by

$$\frac{dV(r)}{d\ln r} = V(r)\frac{dN(r)}{d\ln r} = \frac{4}{3}\pi r^3 \frac{dN(r)}{d\ln r} \text{ and}$$

$$\frac{dA(r)}{d\ln r} = A(r)\frac{dN(r)}{d\ln r} = 4\pi r^2 \frac{dN(r)}{d\ln r}, \text{ respectively.}$$

The effective radius is related to the integral of the ratio between the two:

$$r_{\text{eff}}(\text{total}) = \frac{\int_{r_{\min}=0\mu\text{m}}^{r_{\max}=x\mu\text{m}} r^3 \frac{dN(r)}{d\ln r}\, d\ln r}{\int_{r_{\min}=0\mu\text{m}}^{r_{\max}=x\mu\text{m}} r^2 \frac{dN(r)}{d\ln r}\, d\ln r}.$$

AERONET retrieves volume in each size bin independently, whereas MODIS assumes a superposition of lognormal modes. The lognormal volume distribution is defined as

$$\frac{dV(r)}{d\ln r} = V_0 \frac{1}{\sigma\sqrt{2\pi}} \exp\left[\frac{-\ln(r/r_v)^2}{2\sigma^2}\right],$$

where the median radius r_v and standard deviation σ are defined by

$$\ln r_{v(\text{total})} = \frac{\int_{r_{\min}=0.0\mu\text{m}}^{r_{\max}=x\mu\text{m}} \ln r \frac{dV(r)}{d\ln r}\, d\ln r}{\int_{r_{\min}=0.0\mu\text{m}}^{r_{\max}=x\mu\text{m}} \frac{dV(r)}{d\ln r}\, d\ln r}, \text{ and}$$

$$\sigma(\text{total}) = \sqrt{\frac{\int_{r_{\min}=0\mu\text{m}}^{r_{\max}=x} [\ln r - \ln r_v(\text{total})]^2 \frac{dV(r)}{d\ln r}\, d\ln r}{\int_{r_{\min}=0\mu\text{m}}^{r_{\max}=x} \frac{dV(r)}{d\ln r}\, d\ln r}}.$$

The quantity V_0 is the aerosol column volume per cross sectional surface area. Please see Remer and Kaufman (1998) and Seinfeld (1986, 275–288) for additional derivations.

REFERENCES

Chen, L. W. A., B. G. Doddridge, R. R. Dickerson, J. C. Chow, and R. C. Henry, 2002: Origins of fine aerosol mass in the Baltimore–Washington corridor: Implications from observation, factor analysis, and ensemble air parcel back trajectories. *Atmos. Environ.,* **36,** 4541–4554.

Chu, D. A., Y. J. Kaufman, C. Ichoku, L. A. Remer, D. Tanré, and B. N. Holben, 2002: Validation of MODIS aerosol optical depth retrieval over land. *Geophys. Res. Lett.,* **29,** 8007, doi:10.1029/2001GL013205.

Committee on Extension to the Standard Atmosphere (COESA), 1976: *U.S. Standard Atmosphere, 1976*. U.S. Government Printing Office, Washington, D.C., 227 pp.

Dickerson, R. R., S. Kondragunta, G. Stenchikov, K. L. Civerolo, B. G. Doddridge, and B. N. Holben, 1997: The impact of aerosols on solar ultraviolet radiation and photochemical smog. *Science,* **278,** 827–830.

Dubovik, O., and M. D. King, 2000: A flexible inversion algorithm for retrieval of aerosol optical properties from sun and sky radiance measurements. *J. Geophys. Res.,* **105** (D16), 20 673–20 696.

——, B. Holben, T. F. Eck, A. Smirnov, Y. J. Kaufman, M. D. King, D. Tanré, and I. Slutsker, 2002: Variability of absorption and optical properties of key aerosol types observed in worldwide locations. *J. Atmos. Sci.,* **59,** 590–608.

Eck, T. F., B. N. Holben, J. S. Reid, O. Dubovik, A. Smirnov, N. T. O'Neill, I. Slutsker, and S. Kinne, 1999: Wavelength dependence of the optical depth of biomass burning, urban and desert dust aerosols. *J. Geophys. Res.,* **104** (D8), 31 333–31 349.

Ehsani, A. R., J. A. Reagan, and W. H. Erxleben, 1998: Design and performance analysis of an automated 10-channel solar radiometer instrument. *J. Atmos. Oceanic Technol.,* **15,** 697–707.

Gao, B.-C., Y. J. Kaufman, D. Tanré, and R.-R. Li, 2002: Distinguishing tropospheric aerosols from thin cirrus clouds for improved aerosol retrievals using the ratio of 1.38-μm and 1.24-μm channels. *Geophys. Res. Lett.,* **29,** 1890, doi:10.1029/2002GL015475.

Holben, B. N., and Coauthors, 1998: AERONET—A federated instrument network and data archive for aerosol characterization. *Remote Sens. Environ.,* **66,** 1–16.

Houghton, J. T., Y. Ding, D. J. Griggs, M. Noguer, P. J. van der Linden, X. Dai, K. Maskell, and C. A. Johnson, Eds., 2001: *Climate Change 2001: The Scientific Basis.* Cambridge University Press, 944 pp.

Ichoku, C., D. A. Chu, S. Mattoo, Y. J. Kaufman, L. A. Remer, D. Tanré, I. Slutsker, and B. N. Holben, 2002a: A spatiotemporal approach for global validation and analysis of MODIS aerosol products. *Geophys. Res. Lett.,* **29,** 8006, doi:10.1029/2001GL013206.

——, and Coauthors, 2002b: Analysis of the performance characteristics of the five-channel Microtops II sun photometer for measuring aerosol optical thickness and precipitable water vapor. *J. Geophys. Res.,* **107,** 4179, doi:10.1029/2001JD001302.

——, L. A. Remer, Y. J. Kaufman, R. Levy, D. A. Chu, D. Tanré, and B. N. Holben, 2003: MODIS observation of aerosols and estimation of aerosol radiative forcing over southern Africa during SAFARI 2000. *J. Geophys. Res.,* **108,** 8499, doi:10.1029/2002JD002366.

Kaufman, Y. J., and R. S. Fraser, 1983: Light extinction by aerosols during summer air pollution. *J. Climate Appl. Meteor.,* **22,** 1694–1706.

——, and L. A. Remer, 1994: Detection of forests using mid-IR reflectance—An application for aerosol studies. *IEEE Trans. Geosci. Remote Sens.,* **32,** 672–683.

——, and Coauthors, 1997a: Passive remote sensing of tropospheric aerosol and atmospheric correction for the aerosol effect. *J. Geophys. Res.,* **102** (D14), 16 815–16 830.

——, D. Tanre, L. A. Remer, E. F. Vermote, A. Chu, and B. N. Holben, 1997b: Operational remote sensing of tropospheric aerosol over land from EOS moderate resolution imaging spectroradiometer. *J. Geophys. Res.,* **102** (D14), 17 051–17 067.

——, A. E. Wald, L. A. Remer, B. C. Gao, R. R. Li, and L. Flynn, 1997c: The MODIS 2.1-mu m channel—Correlation with visible reflectance for use in remote sensing of aerosol. *IEEE Trans. Geosci. Remote Sens.,* **35,** 1286–1298.

——, N. Gobron, B. Pinty, J. L. Widlowski, and M. M. Verstraete, 2002: Relationship between surface reflectance in the visible and mid-IR used in MODIS aerosol algorithm—Theory. *Geophys. Res. Lett.,* **29,** 2116, doi:10.1029/2001GL014492.

King, M. D., Y. J. Kaufman, W. P. Menzel, and D. Tanré, 1992: Remote-sensing of cloud, aerosol, and water-vapor properties from the Moderate Resolution Imaging Spectrometer (MODIS). *IEEE Trans. Geosci. Remote Sens.,* **30,** 2–27.

——, and Coauthors, 2003: Cloud and aerosol properties, precipitable water, and profiles of temperature and water vapor from MODIS. *IEEE Trans. Geosci. Remote Sens.,* **41,** 442–458.

Levy, R. C., and Coauthors, 2003: Evaluation of the MODIS retrievals of dust aerosol over the ocean during PRIDE. *J. Geophys. Res.,* **108**, 8594, doi:10.1029/2002JD002460.

Li, R. R., Y. J. Kaufman, B. C. Gao, and C. O. Davis, 2003: Remote sensing of suspended sediments and shallow coastal waters. *IEEE Trans. Geosci. Remote Sens.,* **41,** 559–566.

Malm, W. C., 1992: Characteristics and origins of haze in the continental United-States. *Earth-Sci. Rev.,* **33,** 1–36.

Martins, J. V., D. Tanré, L. A. Remer, Y. J. Kaufman, S. Mattoo, and R. Levy, 2002: MODIS cloud screening for remote sensing of aerosol over oceans using spatial variability. *Geophys. Res. Lett.,* **29,** 8009, doi:10.1029/2001GL013252.

Morys, M., F. M. Mims III, S. Hagerup, S. E. Anderson, A. Baker, J. Kia, and T. Walkup, 2001: Design, calibration and performance of Microtops II handheld ozone monitor and sun photometer. *J.Geophys. Res.,* **106** (D13), 14 573–14 582.

Nakajima, T., G. Tonna, R. Z. Rao, P. Boi, Y. Kaufman, and B. Holben, 1996: Use of sky brightness measurements from ground for remote sensing of particulate polydispersions. *Appl. Opt.,* **35,** 2672–2686.

Parkinson, C. L., 2003: Aqua: An earth-observing satellite mission to examine water and other climate variables. *IEEE Trans. Geosci. Remote Sens.,* **41,** 173–183.

Platnick, S., M. D. King, S. A. Ackerman, W. P. Menzel, B. A. Baum, J. C. Riedi, and R. A. Frey, 2003: The MODIS cloud products: Algorithms and examples from Terra. *IEEE Trans. Geosci. Remote Sens.,* **41,** 459–473.

Redemann, J., and Coauthors, 2005: Suborbital measurements of spectral aerosol optical depth and its variability at subsatellite grid scales in support of CLAMS 2001. *J. Atmos. Sci.,* **62,** 993–1007.

Remer, L. A., and Y. J. Kaufman, 1998: Dynamic aerosol model: Urban/industrial aerosol. *J. Geophys. Res.,* **103** (D12), 13 859–13 871.

——, A. E. Wald, and Y. J. Kaufman, 2001: Angular and seasonal variation of spectral surface reflectance ratios: Implications for the remote sensing of aerosol over land. *IEEE Trans. Geosci. Remote Sens.,* **39,** 275–283.

——, and Coauthors, 2002: Validation of MODIS aerosol retrieval over ocean. *Geophys. Res. Lett.,* **29,** 8008, doi:10.1029/2001GL013204.

——, and Coauthors, 2005: The MODIS aerosol algorithm, products, and validation. *J. Atmos. Sci.,* **62,** 947–973.

Russell, P. B., and Coauthors, 1993: Pinatubo and pre-Pinatubo optical-depth spectra: Mauna Loa measurements, comparisons, inferred particle size distributions, radiative effects, and relationship to lidar data. *J. Geophys. Res.,* **98,** 22 969–22 985.

Samet, J. M., F. Dominici, F. C. Curriero, I. Coursac, and S. L. Zeger, 2000: Fine particulate air pollution and mortality in 20 US Cities, 1987–1994. *New Engl. J. Med.,* **343,** 1742–1749.

Seinfeld, J. H., 1986: *Atmospheric Chemistry and Physics of Air Pollution.* John Wiley and Sons, 738 pp.

Smirnov, A., B. N. Holben, T. F. Eck, O. Dubovik, and I. Slutsker, 2000: Cloud-screening and quality control algorithms for the AERONET database. *Remote Sens. Environ.,* **73,** 337–349.

Smith, W. L., Jr., T. P. Charlock, R. Kahn, J. V. Martins, and L. Remer, 2005: EOS-TERRA aerosol and radiative flux validation, 2004: An overview of the Chesapeake Lighthouse and Aircraft Measurements for Satellites (CLAMS) experiment. *J. Atmos. Sci.,* **62,** 903–918.

Tanré, D., M. Herman, and Y. J. Kaufman, 1996: Information on aerosol size distribution contained in solar reflected spectral radiances. *J. Geophys. Res.,* **101** (D14), 19 043–19 060.

——, Y. J. Kaufman, M. Herman, and S. Mattoo, 1997: Remote sensing of aerosol properties over oceans using the MODIS/EOS spectral radiances. *J. Geophys. Res.,* **102** (D14), 16 971–16 988.

Vermote, E. F., N. El Saleous, C. O. Justice, Y. J. Kaufman, J. L. Privette, L. Remer, J. C. Roger, and D. Tanré, 1997a: Atmospheric correction of visible to middle-infrared EOS-MODIS data over land surfaces: Background, operational algorithm and validation. *J. Geophys. Res.,* **102** (D14), 17 131–17 141.

——, D. Tanré, J. L. Deuze, M. Herman, and J. J. Morcrette, 1997b: Second simulation of the satellite signal in the solar spectrum, 6S: An overview. *IEEE Trans. Geosci. Remote Sens.,* **35,** 675–686.